Scanning Microscopy Vol. 11, 1997 (Pages 345-366) 0891-7035/97$5.00+.25
Scanning Microscopy International, Chicago (AMF O'Hare), IL 60666 USA

SELECTED TOPICS IN CHARGED PARTICLE INTERFEROMETRY

Franz Hasselbach

Institut für Angewandte Physik der Universität Tübingen, Tübingen, Germany

Abstract

Following a short survey on the early developments in particle diffraction, interferometry and holography, the constructional details and advantages of our novel miniaturized low voltage biprism interferometer are presented. As a unique electron optical component in an interferometer, a crossed field analyzer (Wien-filter) is included in the beam path. Inside the crossed field analyzer the wave packets propagate on laterally separated paths of different electric potential and in turn with different group velocities provoking a relative longitudinal shift along the beam path of the self interfering two wave packets at the exit plane of the crossed field analyzer. The value of this shift can be chosen to any extent desired by varying of its excitation. Varying this longitudinal shift corresponds to a variation in longitudinal coherence of the ensemble of electrons.

The new interferometer enabled us to realize the following experiments: proof of the rotationally induced phase shift of electron waves (Sagnac-effect), study of phase shifts of electron waves by electromagnetic fields and longitudinal shifts of wave packets by electrostatic fields, coherence length measurements, and visibility spectroscopy (Fourier-spectroscopy) of electron waves. After reporting extensively on these experiments our new studies in progress are discussed: Development of an ion biprism interferometer with a high brightness field ion source, antibunching of electron waves and a high brightness polarized field electron source with presumably very attractive properties for electron microscopy, electron interferometry and scanning tunneling microscopy.

Key Words: Electron interferometry, Aharonov-Bohm phase differences, Sagnac effect, coherence length, Fourier spectroscopy, ion interferometry, electron antibunching, polarized electron source.

*Address for correspondence:
Franz Hasselbach
Institut für Angewandte Physik der Universität Tübingen
Auf der Morgenstelle 12, D-72076 Tübingen, Germany
Telephone number: +49-7071-2976328
FAX number: +49-7071-295400
E-mail franz.hasselbach@uni-tuebingen.de

Introduction

Early developments in particle diffraction, interferometry and holography

Diffraction and interferometry of particles, especially of electrons, have been firmly established for the past seventy years. As early as 1925, Elsasser [34] realized that in single crystals, nature provided us with almost perfectly aligned interferometers for matter waves. Experimental difficulties caused a two year delay between his suggestion and realization in the experiment in 1927 by Davisson and Germer [26]. For their diffraction experiment with electrons, periodically arranged nickel atoms of a single crystal were used. It was the first experimental proof of the wave particle duality hypothesis established theoretically in duc de Broglie's thesis in 1924 [27, 28, 29] and of Schrödinger's, Heisenberg's and Dirac's revolutionary theories governing the microscopic world: Quantum mechanics. As early as 1930, Estermann and Stern [35] reported diffraction of neutral helium atoms by lithium fluoride crystals and in 1940 the first diffraction experiment of electrons by macroscopic obstacles has been successfully realized by Boersch [8, 9, 10] in an electron microscope. Unknowingly, Boersch's diffraction patterns, produced simply by defocusing his microscope under conditions of relatively high coherence of the illuminating beam, were the first in-line holograms taken. Between 1948 and 1951, Dennis Gabor introduced in three fundamental papers [41, 42, 43] his "microscopy by diffracted wavefronts" or "diffraction microscopy" in order to overcome the limitations of the electron microscope caused by geometric aberrations of the electron lenses in a roundabout way. The projection method of diffraction microscopy as originally proposed by Gabor proved to have the major disadvantage of requiring very long exposure times of the order of 30 minutes of the holograms. [*Note*: However, this has changed completely when field emission guns became available with their up to 10^4 times more brightness.] Gabor's scheme has been shown to be viable both for resolution enhancement [72] and for the study of magnetic fields [75]. Even today's state of the art microscopes are not stable enough to allow such long exposure times. It has been replaced by the "transmission method" of Haine and Dyson [46] in 1950, which consists simply of taking a defocused image of the microscopic object. The

experimental realization of this type of electron holography was in the hands of M.E Haine and T. Mulvey extremely successful: in their own words [47]. In our experiments, by paying careful attention to mechanical stage design and general instrument stability both mechanical and electrical, we have so far been able to obtain a resolution of 5-6 Å in the diffraction image. And V.E. Cosslett commented at the same conference on Haine and Mulvey's experiments "It is claimed that a resolution of about 10 Å has been obtained already, the limitation at the moment being as much in the reconstruction procedure as in the actual electron microscopy" and "It is encouraging that this new method has already reached the same level of resolution as straight electron microscopy, but it appears that it is liable to be limited in the end by much the same factors: The instabilities of the instrument, rather than the aberrations of the lenses. But if these mechanical and electrical problems can be solved, it holds out a clear prospect of circumventing spherical aberration and so allowing a resolution of atomic order to be achieved" [19]. It is worth mentioning here that this remarkable success has been reached nearly ten years before the invention of the laser. The holograms had to be reconstructed using light from an arc lamp monochromatized by interference filters.

At the same time work was in progress in the United States and Germany to build an electron interferometer in close analogy to the interferometers of light optics. To make a long story short, the group around L. Marton tried to realize a beam splitter by the use of diffraction on thin crystal lamellae [75, 76, 77, 117, 118] (amplitude splitting) and Möllenstedt and Düker succeeded in 1954 in the development of the biprism for electrons [36, 83, 84] (wavefront splitting). The latter became the standard versatile beam splitter of variable strength in electron interferometers and electron holography microscopes while Marton's amplitude splitting device has turned out to be the best choice for neutron interferometers [99].

This developmental phase of electron interferometry/holography was followed by one concerned with its application for measurement purposes and questions of purely fundamental interest: Fresnel diffraction by circular diaphragms by Faget and Fert [36], determination of mean inner potentials [85] in solids by interference microscopy [14, 36] or the phase shifts of electron waves by a magnetic flux [1, 33, 39, 40, 93] enclosed between the coherent beams were typical applications [5, 12, 16, 82, 122] in these early days. The Brno-group, J. Komrska, V. Drahos and A. Delong [32, 68, 69, 70] contributed a consistent theoretical interpretation of the electron interference phenomena produced by an electrostatic biprism and demonstrated the validity of their model by impressive experimental and calculated interference patterns.

At the end of the sixties, the efforts of Möllenstedt and Wahl, Tonomura and Tomita *et al*. to realize off-axis holography were successful [86, 119, 120]. At about the same time high brightness, highly coherent field emission cathodes were introduced into electron microscopy by A.V. Crewe [23, 24]. Simultaneously, the first electron interferometer with such a field emitter was built by W. Brünger [13] in Tübingen. This new, by many orders of magnitude, brighter and coherent electron source opened the gateway to the development of a new generation of electron microscopes, triggered electron holography and experiments which were absolutely inconceivable with the old thermionic cathodes. In atom interferometry Leavitt and Bills succeeded in seeing single-slit diffraction patterns of a thermal atomic potassium beam in 1969 [71]. I want to conclude this short and by no means complete survey. The developments in the field with the new type of microscopes may be found, e.g., in review papers of Missiroli *et al*. [81], Olariu and Popescu [91], Tonomura [121, 123] and are one subject of this conference. The latest results and references may be found in other contributions to this volume.

Motivation for developing a new type of electron interferometer

As already mentioned in the introduction, field emission and highly stable power supplies, which became available owing to advances in microelectronics, caused a jump in the resolution of electron microscopes. A.V. Crewe's scanning transmission microscope (STEM) as well as conventional transmission electron microscopes (TEMs) resolved atoms routinely in the mid-seventies [2]. However, some deficiencies remained largely unsolved: The sensitivity to mechanical vibrations, the mechanical and electrical long term stability and sensitivity to alternating electromagnetic fields. Even today, these deficiencies exist even in the most advanced electron microscopes. Due to instabilities, exposure times of atomic resolution micrographs exceeding minutes are not possible. Switching off fluorescent lights and avoiding any mechanical disturbances even by speaking during exposure are a must. Surprisingly, the well established constructional principles have not been called into question, the constructional deficiencies just mentioned are still present.

When entering into the field of electron interferometry in the mid-seventies one of the goals was to construct an electron interferometer, with which the rotationally induced phase shift (Sagnac effect) of electron waves could be measured. An electron interferometer, which is inherently far more insensitive to the disturbances mentioned, i.e., which can be operated in virtually every environment and which is small enough to be easily mobile, is indispensable, since for this experiment the whole interferometer has to be rotated on a turntable. This was the starting point for constructing a new interferometer totally different in design from the conventional ones which are usually modified

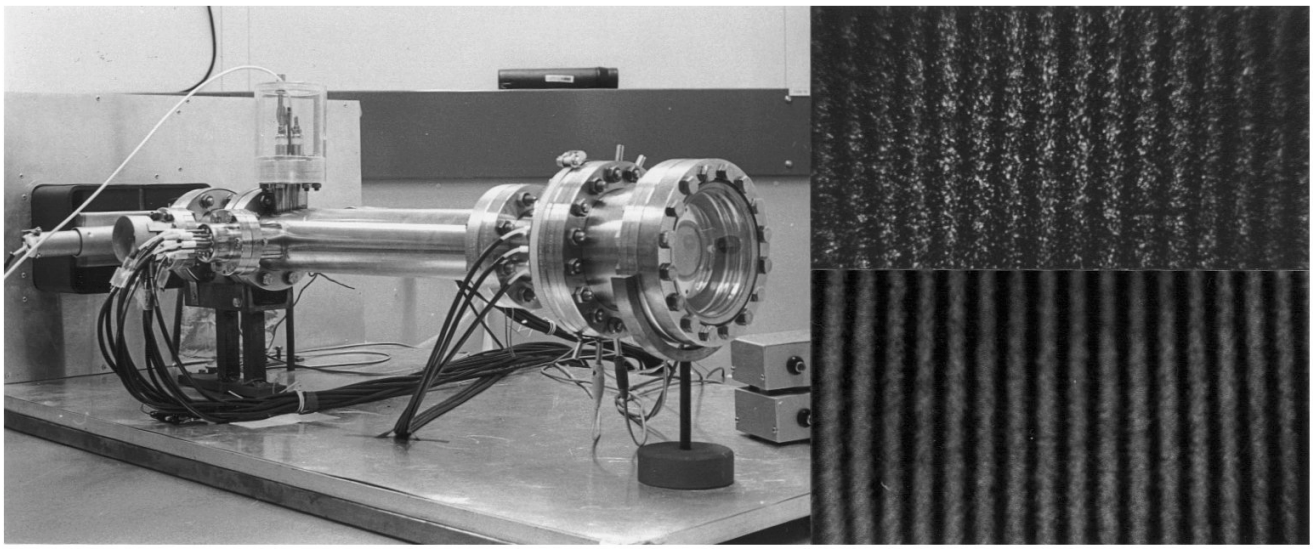

Figure 1. Left: Outside view of the interferometer. Top right: At very low emission of the cathode the arrival of single electrons becomes visible on the fluorescent screen of the image intensifier. The bright spots demonstrate the particle properties of the electrons, their arrangement in fringes their simultaneously present wave properties. Bottom right: High emission. Interference fringes are clearly visible.

electron microscopes.

Constructional Details and Advantages of the New Interferometer

The first interferometer of the new type went into operation in 1979 [53], and showed that the design goals had been reached. A detailed publication of the state of the art in 1980 was only published in 1988 [54], shortly before the successful completion of our Sagnac experiment with electron waves [57], which is the most crucial demonstration of its exceptional new qualities compared to conventional instruments. An outside view of the interferometer is given in Figure 1. On the right-hand side the build-up of an interference pattern out of single events is demonstrated.

The mechanical and electron optical set-up of the new type of interferometer are given in Figures 2a and b; the beam path for a three-biprism arrangement with coherent beams separated by about 100 μm is shown in Figure 2c (a separation, i.e., an enclosed area between the coherent beams is necessary, e.g., when an Aharonov-Bohm or a Sagnac-experiment is planned). Low-energy electrons (150 eV to 3 keV) emitted from a field-emission diode electron gun are used. The electrostatic deflection systems are used for fine alignment of the electron beam onto the axis of the electron optical components. The coherent wavefronts are made to diverge by a negatively charged filament [5], then to converge by a second positively charged one. The third, negatively charged biprism reduces the angle of superposition of the coherent wavefronts leading to a larger spacing of the fringes in the primary interference plane. The wave fronts leaving the first and second biprism may be slightly rotated by weak longitudinal homogeneous magnetic fields (produced by the alignment coils) in order to align them with the direction of the following biprism filament.

In summary:

The electron source is a field emission gun; it is a simple diode system without any additional acceleration voltage.

Very low electron energies in the range of 150 eV to 3 keV are used.

Only electrostatic lenses and deflection elements are used with one exception: for aligning the direction of the wavefronts in multiple biprism arrangements homogeneous magnetic fields are utilized.

The optical elements are very small and fabricated to a high degree of precision: outer diameter 28 mm ± 10 μm.

A very rigid optical bench consisting of two ceramic rods of excellent straightness and constancy in diameter (± 10 μm) is used onto which the optical elements are tightly fixed by a brace construction. The possibility of vibration of the elements relative to each other is thus minimized.

The mechanical eigenfrequency of the interferometer is so high that it cannot be excited by low frequency vibrations coming along the floor of the building. Furthermore, this construction principle ensures an excellent prealignment. Therefore, no mechanical alignment facilities are necessary.

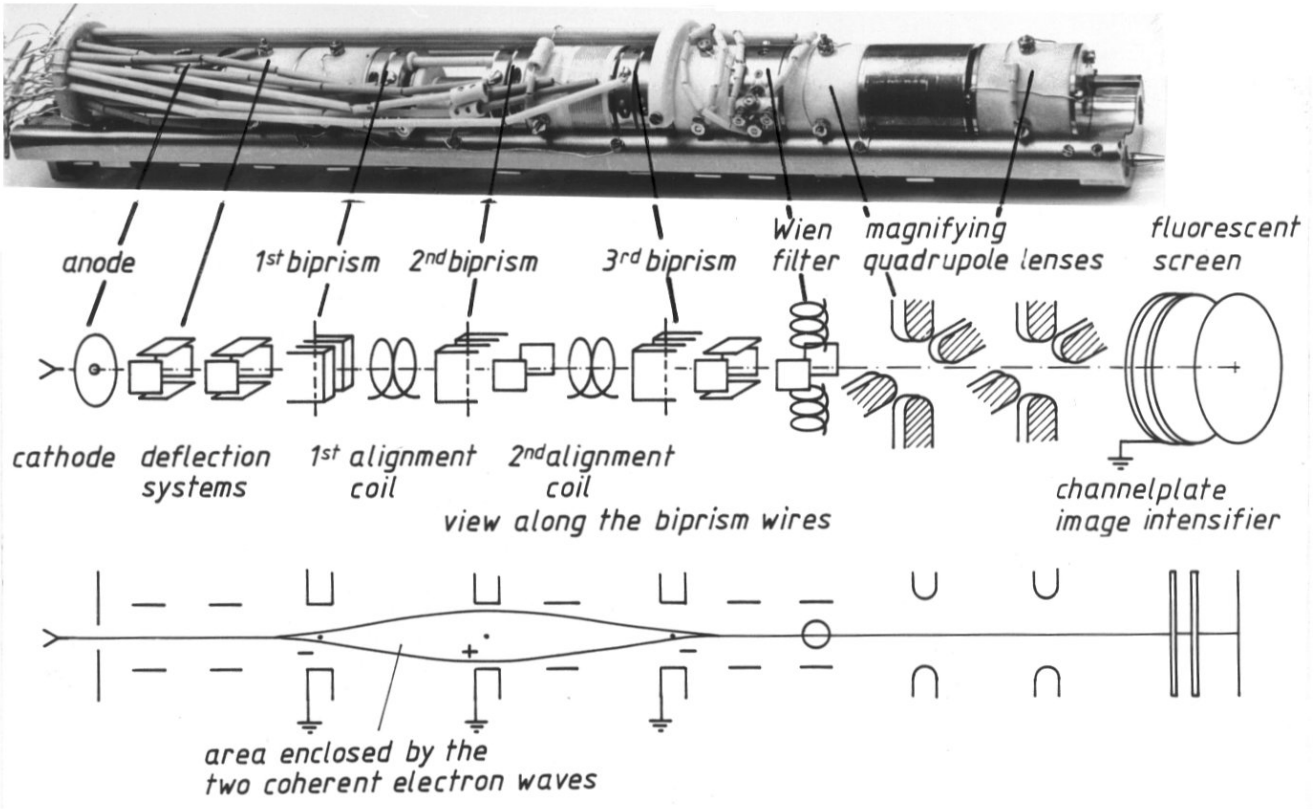

Figure 2. Miniaturized biprism interferometer. Top: View of electron optical components (diameter 28 mm) tightly fixed on a miniaturized optical bench (total length 30 cm) consisting of two precision ceramic rods. The image intensifier is about 20 cm away from the second magnifying quadrupole lens. Center: Schematical set-up. Bottom: Beam path (by three biprisms a larger enclosed area between the coherent beams is realized, e.g., for the Sagnac experiment).

Only electric and magnetic fine alignment are needed and provided. Therefore, no mechanical feedthroughs with their detrimental effect on the magnetic shielding are necessary.

A nearly complete, very effective magnetic shielding by a high permeability cylinder without lateral bores is possible (shielding factors $\geq 10^4$ with a single walled cylinder).

Materials used:

For the electron optical components: Titanium (completely unmagnetic), machinable glass ceramics as an insulator. Both materials have very similar expansion coefficients which is essential for baking. Electrical shields: Copper.

A single optical element (crossed beam analyzer, Wien filter) allows one to shift charged particle wave packets longitudinally.

The new electron optical bench system has been successfully used by other colleagues [6] in the institute and worked well up to voltages of 20 keV.

The primary interference fringes are magnified by quadrupole lenses, intensified by a dual-stage channelplate image intensifier and transferred to a charge-coupled device (CCD)-camera by fiber optics and evaluated by an image processing system. The entire interferometer may be powered by batteries. It can sit up on a turntable (including all power supplies and batteries) in order to measure the influence of inertial potentials and fields on the phase of the electron waves. The interference fringes are transmitted by a slip ring to the laboratory frame.

Influence of Inertial Potentials and Forces on the Phase of Electron Waves (Sagnac Experiment)

The Sagnac experiment for electron waves, together with the Sagnac experiments for neutrons and neutral atoms, demonstrates that the coupling of inertial potentials and forces (fields) is independent of the charge. We do not want to go into details of these questions here; they may be found in special publications [57, 62, 90, 94, 100, 125]. However, a short explanation of the Sagnac-effect for massive particles which is not as well known as the Sagnac-

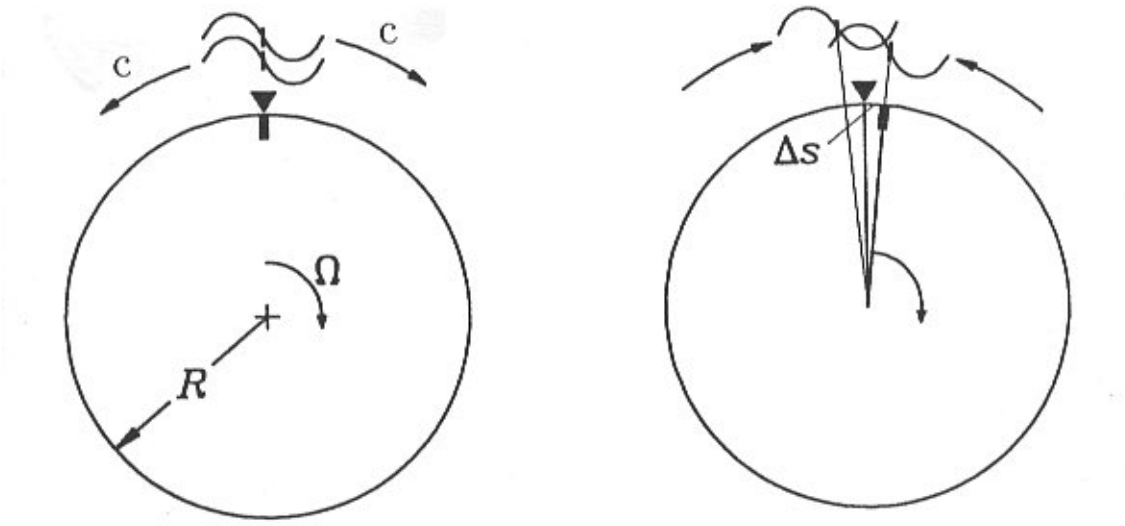

Figure 3. Principle of the Sagnac interferometer. Coherent light waves start at point S which is marked in the laboratory frame by a triangle and in the rotating frame by a quadrangle. They go around the same closed circular path with radius R in opposite directions, enclose an area $\vec{A}$ and interfere when they meet again. When the interferometer is not rotating, they are in phase. If it is rotating, the co-rotating detector has moved a short distance to the right on arrival of the counter-clockwise (CCW) wave, i.e., the path length for the CCW wave to the detector is shorter, that of the clockwise (CW) wave longer. This translates into the rotationally induced Sagnac phase shift of the waves in the detector plane.

effect for photons may be appropriate here. In a Sagnac interferometer radiation from a source is split into two coherent beams, encircles an enclosed area and interferes thereafter. The phase shift $\Delta\phi$ caused by rotation of the interferometer is proportional to the enclosed oriented area $\vec{A}$, the rotation rate $\vec{\Omega}$ and the total energy E (kinetic energy + rest mass) of the quanta of radiation $\Delta\phi = (8\pi/hc^2)\, E\vec{A}\vec{\Omega}$.

The optical effect is easily understood: The speed of light c is independent of the speed of the emitting source and equals c in both directions. In order to be specific, let us assume that the turntable with our interferometer is rotating clockwise (CW). Due to the rotation, the path length for the photons to the detector emitted in CW direction is longer than that for the counter-clockwise (CCW) shorter. It differs by $2\Delta s = 4R\Omega(\pi R/v)$. This path length difference divided by the wavelength of the photons is the Sagnac phase shift.

(1)

$$\Delta\phi = \left(\frac{2\Delta s}{\lambda}\right)2\pi = 4R\Omega\frac{\pi R}{c} = \left(\frac{8\pi}{\lambda c}\right)\vec{A}\vec{\Omega} = \left(\frac{8\pi}{hc^2}\right)E\vec{A}\vec{\Omega} = \frac{4}{\hbar}m\vec{A}\vec{\Omega}$$

By substituting $\lambda = h/p = h/mv$ and $E=mc^2$ one gets the right hand side term in Equation (1) which is the Sagnac phase shift for matter waves.

Massive particles leave the source with velocity $v+\vec{\Omega}r$ (CW) and $v-\vec{\Omega}r$ where v is the velocity of their emission for zero rotation rate. By applying a Galilei transformation we can calculate the arrival times of, e.g., electrons at the detector in the rotating frame and the laboratory frame. Due to the assumption of an absolute time in classical physics, the calculated arrival times in both frames are identical. Consequently, there is no Sagnac effect in classical physics. As a prerequisite to explain the Sagnac effect additional nonclassical ingredients are needed: Relativity of time and the wave nature of particles, more specifically phase differences of particle waves. The first is given to us by the theory of relativity and the second by quantum mechanics. One of a number of possibilities to explain the Sagnac effect is as follows: It is well known (and experimentally proven in π meson experiments) that ageing is less in high speed travel because of the relativistic time dilatation phenomenon. A consequence of this phenomenon is, in every day life, the strange clock paradoxon, i.e., a pair of clocks (corresponding to wave packets) travelling clock- and counterclockwise around the rotating disk show different times on arrival at the detector. Their time difference corresponds to a phase difference, the Sagnac phase shift. This explanation of the Sagnac effect for massive particles demonstrates that the origin of the effect is purely relativistic. It is remarkable that the Sagnac phase difference is independent of the speed of the signals (nondispersive) and depends on the angular velocity and the enclosed area only. From the point of view of rotation sensing it is the physical effect predestined for

that purpose. While all variables return to their original values after encircling the area, the phase does not (phase anholonomy) and instead gives rise to a shift of the interference fringes. In the parlance of geometrical and topological anholonomies (Berry phases) the Sagnac effect for massive particles is due to an age anholonomy (twin paradoxon) which corresponds a phase anholonomy when the twins are replaced by interfering particles [17]. It is remarkable that nonrelativistic quantum mechanics predicts the Sagnac phase difference correctly, which demonstrates that nonrelativistic quantum mechanics is not in all respects a Galilean invariant theory [30, 31].

To perform the Sagnac experiment the whole interferometer was fixed on a turntable and put into CW and CCW rotation three times in each experiment at frequencies of up to 1 Hz. [*Note*: The beam path in the present Sagnac experiment is given in Figure 2, bottom. It differs from "conventional" Sagnac interferometers (see, e.g., Fig. 3) where starting and interference plane coincide, i.e., the beams travel a full closed loop: In the present experiment the coherent beams travel semicircular paths only before they interfere. Consequently the values of the phase shifts are 50% of those given in Equation (1). Sagnac phase shifts are found in rotating interferometers when an effective area $\bar{A}$ is enclosed by the coherent beams.] The experiment is performed on the seventh floor of the building. No vibration damping was provided. The wavelength of the electrons in our Sagnac experiment was about 0.1 Å. The duration of one experiment was typically about 20 minutes. The phase shift caused by the CW and CCW rotations was $\leq 6\%$ of a fringe width. In order to limit the error bars in the experiment to less than 15%, the sum of all errors (mechanical and electrical instabilities, drift) must not exceed 1% of a fringe width during the total duration of an experiment of 20 minutes. It turned out that the limiting factor of the present interferometer was not the mechanical and electrical stability but the instabilities of the field emission. Nevertheless, the stability achieved with the new design of electron optical instruments exceeds that of conventional microscopes by at least one order of magnitude (A new high resolution field emission scanning electron microscope on the same floor achieves its resolution limit only during the night when the disturbances are low).

From the point of view of electron microscopy the extraordinary stability of the new design of an electron interferometer is of interest. The fact that its design can easily be adapted to solve other problems is the reason for presenting its features as exemplified by the crucial Sagnac experiment.

Influence of Electromagnetic Potentials and Fields on Trajectories and Phase of Electron Wave Packets - the Crossed Field Analyzer (Wien Filter): A Wave Packet Shifting Device for Charged Particles

In 1979, Möllenstedt and Wohland discovered a wave-packet-shifting device in the form of a Wien filter (crossed electric and magnetic fields, "crossed field analyzer") and measured the coherence length of electron waves [87, 126].

A brief outline of the action of the Wien filter on electron wave packets is given in Figure 4. A Wien filter consists of crossed electric and magnetic fields, both perpendicular to the beam path. The Wien filter is said to be in its *compensated state* when the electric and magnetic forces on the charged particles just cancel each other, i.e., the trajectories of the particles are not affected by the electromagnetic fields in the Wien filter. For the case of the compensated Wien filter it can be shown easily (see, e.g., [55, 89]) that the phase shifts exerted by the electric and magnetic potentials are opposite to each other and of exactly the same magnitude. [*Note*: Electric and magnetic Aharonov-Bohm phase shifts [1, 93]. The magnetic flux enclosed by the coherent beams creates a certain phase shift which is exactly compensated by the phase shift which arises due to the fact that the coherent wave packets travel inside the Wien filter on paths of different electric potential. In essence, by taking into account the well known experiments which prove the magnetic Aharonov-Bohm effect, we have here an indirect proof of the existence of the electric Aharonov-Bohm effect.] In other words: The electron optical index of refraction equals 1 (to first order) inside and outside of the Wien filter. Therefore, in Figure 4 the planes of equal phase (e.g., crests) of the electron waves, represented by the horizontal lines, and the phase velocity are not affected at all by the electromagnetic fields in the *compensated* Wien filter, irrespective of its excitation. [*Note*: The lines of constant phase in all schematic diagrams do not represent reality but only one of an infinite number of possible equivalent descriptions. Quantum-mechanically, phase differences and the corresponding fringe spacings only are elements of reality [97, 98].]

This means that when we increase the excitation of the Wien filter while always maintaining the compensated state, we observe in the observation plane a stationary field of interference fringes, *but*, with increasing excitation of the Wien filter, the fringe contrast decreases continuously due to the fact that the electron wave packets travel on paths of different electric potential with different group velocities inside the Wien filter. This leads to a longitudinal shift of the wave packets at the exit plane and consequently to a reduced contrast of the interference fringes. [*Note*: The

electric potential difference on the two paths increases with increasing excitation of the Wien filter. The acceleration and deceleration of the wave packets to the value inside the Wien filter occurs in the electric fringing fields of the Wien filter condenser.] For longitudinal shifts larger than the coherence length, the fringe contrast vanishes. The contrast or, in the terminology of A.A. Michelson, the visibility V of the fringes as a function of the longitudinal shift x is defined by

$$V(x) = \frac{I_{max}(x) - I_{min}(x)}{I_{max}(x) + I_{min}(x)} = G_1 \cdot G_2 \qquad (2)$$

and equals the product of the spatial (G_1) and temporal (G_2) coherence functions [61]. For coherence length measurements the fringe spacings are chosen so large that G_1=1 by applying a suitable voltage to the biprism filament .

It is important to emphasize the fact that the *Wien filter in its compensated state is not a phase shifter*. The wave packets are shifted longitudinally in a stationary "phase wave sea". The phase of the wave packets is not affected at all when traveling through the electromagnetic fields in a compensated Wien filter.

Refinement of a Wien filter to a high precision retarding device for wave packets

The delay or longitudinal shift caused by a Wien filter can be adjusted with a precision of a small fraction of a wavelength provided that first, the Wien filter construction allows one to adjust the electromagnetic fields in very fine steps and second, that it is aligned to its compensated state in a two-step process [25, 55, 58] (Fig. 5): At first, the magnetic and electric fields are zero. The full overlap of the wave packets corresponds to maximum fringe contrast. Now we increase in a first step the electric field only (left hand side in Fig. 5). The Wien condenser works as a deflection element. It produces a fringe displacement, say, to the left by 6 fringe widths, which exactly keeps pace with the deflection of the beams by the field, so that the fringe system appears to remain undisplaced relative to the envelope of the pattern (Fig. 5 bottom). The phase shift caused by path length difference Δ_1 from the two virtual electron sources to the zero-order fringe in the center of deflected the pattern must be exactly compensated by different indices of refraction (different phase velocities of the coherent waves on their path to the zero-order fringe) or in another terminology, by different Aharonov-Bohm phase shifts. Otherwise the fringes in the deflected pattern would be shifted relative to the undeflected one. On the other hand, group and phase velocity in the electrostatic deflector obey the relation $v_g v_p = c^2$. That is, a higher phase velocity in the Wien filter corresponds to a lower group velocity and vice versa. For the

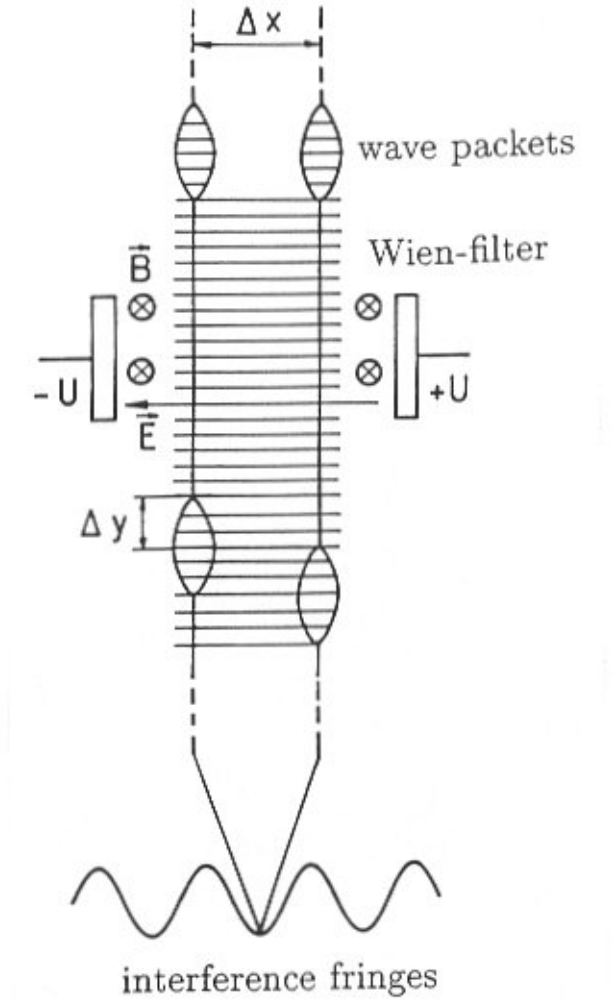

Figure 4. The influence of a Wien filter in its compensated state on two spatially separated electron wave packets. The left-hand side wave packet travels inside the Wien filter on a more negative potential than the right-hand side one, i.e., with a lower group velocity.

zero-order fringe in the deflected pattern the wave trains are in phase, but the geometrical longitudinal shift of the wave packets is made up by the path length difference Δ_1 and the difference caused by the delay due to the lower group velocity which equals Δ_1. Consequently, the overlap of the wave packets at the zero-order fringe in the electrostatically deflected pattern is reduced by 12 wavelengths with the corresponding effect on the con-trast of the pattern (Fig. 5, bottom left). In the second step, the magnetic field of the Wien filter is increased until the deflection due to the electric field is just compensated. The electrostatic and magnetic Aharonov-Bohm phase shifts now exactly compensate each other.

However, the longitudinal shift of 6 fringe widths or

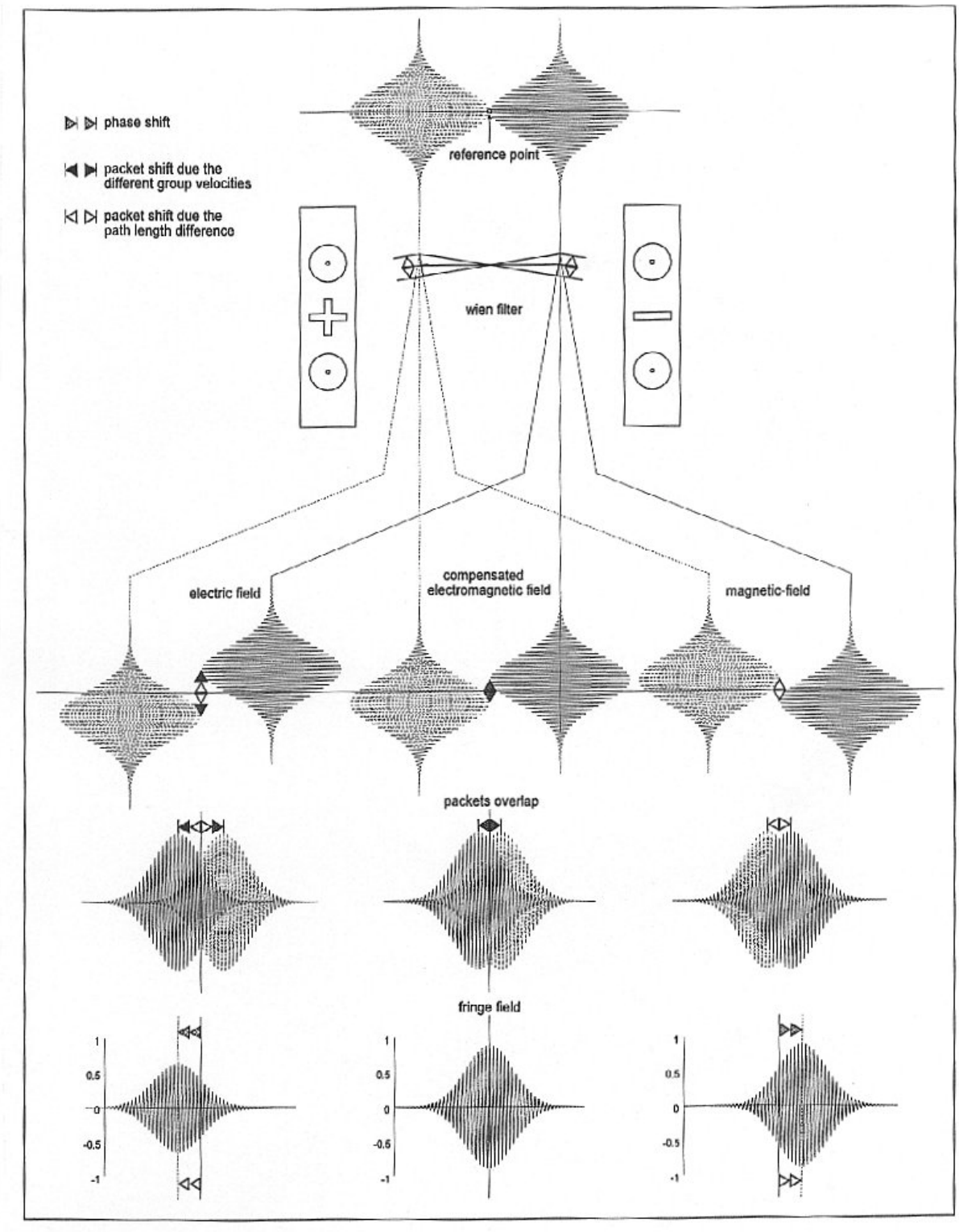

Figure 5. Phase- and group- velocities in electromagnetic fields. The two-step process to reach the compensated state of the Wien filter. In the compensated state (middle of Fig. 5) no deflection occurs and consequently path length differences are zero. The longitudinal shift of the wave packets is due to different group velocities in the laterally separated paths in the Wien filter.

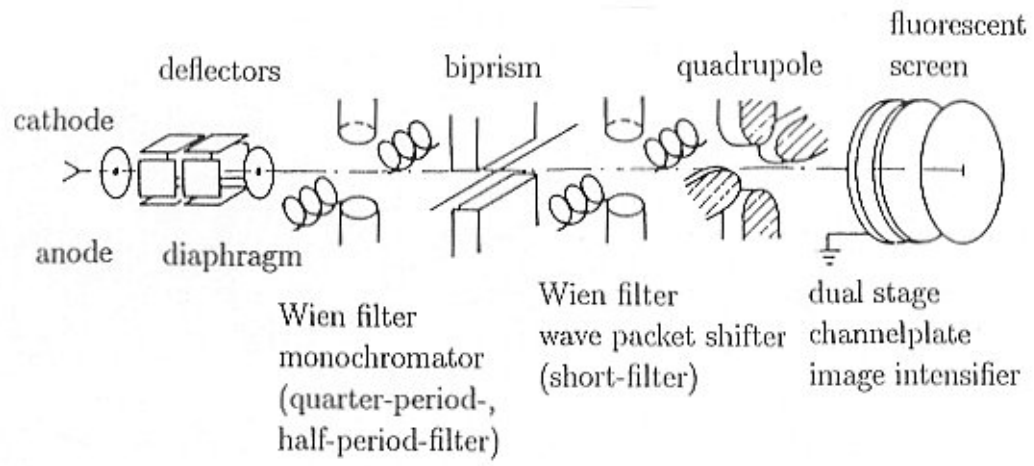

Figure 6. Set-up for measuring of the coherence length as a function of the energy width of the electron beam. The first Wien filter acts as a monochromator, the second one as a wave packet shifting device.

Table 1. Coherence length measurements of field emitted electrons.

author	accelerating voltage	contrast ca.	fringes $N_{fringes}$	coherence length L_c $L_c = N_{fringes}.\lambda_{deBroglie}$	ΔE_{FWHM} (m) measured (c) calculated
Daberkow *et al*. [25]	4000 V	1/e	21800	420 nm	0.43 eV (m)
Schäfer [58, 106]	2000 V	20%	11180	300 nm	0.61 eV (m)
Wachendorfer [125]	2400 V	20%	12320	310 nm	0.59 eV (m)
Bauer [3, 4]	1700 V	10%	21300	640 nm	0.29 eV (c)
Bauer [3, 4]	1700 V	10%	39620	1189 nm	0.16 eV (c)

6 wavelengths of the wave packets due to the different group velocities survives. Consequently the contrast of the fringe pattern after this two step process corresponds to a reduced overlap of the wave packets by 6 wavelengths.

Let me mention here that this measurement method works irrespective of any knowledge of the size of the field strengths and (in-)homogenities of the electromagnetic fields in the Wien filter, not to mention that of the fringing fields. It therefore is intrinsically extremely precise and enables us to measure the longitudinal shift exerted by the Wien filter with a precision of the order of 1% of a wavelength or less. This high precision is a prerequisite to realize Michelson's visibility technique and Fourier spectroscopy for matter waves.

Applications of the Wien Filter

Measurement of coherence lengths of electron waves

The coherence length measurements of our group are summarized in Table 1.

In order to measure coherence lengths [7, 18, 67], the wave packets and their identical replicas are superimposed with different longitudinal shifts until the contrast C of the interference fringes is reduced to, e.g., 1/e, 20% or 10% of its maximum value. In the first column the authors are given. The second contains the acceleration voltage of the electrons followed by the contrast limit C. Fringes with contrast lower than C were neglected. The coherence lengths given in Table 1 are the products of the total number of fringes with C $\geq$ this contrast limit times the wavelength. The full width at half maximum (FWHM) of the spectral distribution given in Table 1 has been measured (m) by visibility spectroscopy or calculated (c) from the measured coherence lengths assuming symmetrical Gaussian distributions of the spectral lines.

Only recently has the increase in coherence length by monochromatization of an electron beam been

demonstrated experimentally [3, 4] (see last two lines of Table 1). The experimental set-up (Fig. 6) consists of an interferometer equipped with a first Wien filter for monochromatization and a second one working as a wave packet shifter.

Interferometric measurement of charged particle spectra (Fourier-spectroscopy)

Classical charged particle spectrometers exploit on the fact that particles with different energies follow different individual trajectories. Different arrival sites in the plane of observation correspond to different energies of the particles. The quantum mechanical counterpart of such a classical measurement is to extract the particle spectrum from the corresponding spread of the de Broglie wavelengths of the ensemble of particles that make up the wave packet. By wavefront or amplitude division, two coherent wave packets are generated. Then, a gradual alteration in the difference in path is introduced between the two interfering streams of electron wave packets. The flux of radiation as a function of the path difference between the beams arriving at the detector contains a constant term and an oscillating one, the interferogram. The interferogram, i.e., the contrast and the spacings of the interference fringes as a function of the path-length difference between the beams characterizes the incident spectrum that produces it, and is analyzed to yield the unique spectral distribution of the radiation reaching the detector. The salient point of this type of spectroscopy compared to trajectory based spectrometers is that imperfections of the optical components do not diminish the clearness of the interferogram if the fringe spacing is chosen sufficiently large. Consequently, their aberrations do not affect and limit the attainable resolution of this new type of charged particle spectrometer. The advantages of this technique cannot be summarized better than A.A. Michelson did in his seminal papers [78, 79, 80] on this subject in 1892, at that time for photons: "The principal object of the foregoing work is to illustrate the advantages which may be expected from a study of the variations of clearness of interference fringes with increase in difference of path. The fundamental principle by which the "structure" of a line or a group of lines is determined by this method is not essentially different from that of spectrum analysis by the grating, both depending, in fact, on interference phenomena; but in consequence of the almost complete freedom from errors arising from defects in optical or mechanical parts, the method has extraordinary advantages for this special work."

In his experiments A.A. Michelson took into account only the visibility of the interference fringes V(x) as a function of the path length difference x and neglected the slight variations of their spacings. Spectral lines that appeared as singlets in ordinary spectrometers are revealed in fact to be doublets or multiplets. However, neglect of the slight variations of the average fringe distances as a function of the longitudinal shift in the interferogram restricted Michelson's visibility technique to spectra symmetric about the center frequency. The complete information encoded in an interferogram was used for the first time by Rubens and Wood for spectral analysis in the far infrared region [104] of the electromagnetic spectrum.

The interferogram. Features of the spectrum of the radiation (the full width at half maximum, the symmetry of the spectral line) are encoded in the interferogram in a characteristic way. This is demonstrated in the following computer simulation of an interferogram (Fig. 7a). In Figure 7b an experimental electron interferogram corresponding to the simulated one of Figure 7a is given. The interferograms shown in Figures 7a and b correspond to a spectrum consisting of two lines of equal intensity. The envelope of the contrast of the fringes is determined by the widths of the lines, while distance of the contrast minima in the fringe pattern is determined by the difference in frequency Δ of the two lines. Since the two lines are of equal intensity, this spectrum can be regarded as a symmetric spectrum. It can be shown that, for symmetric spectra, the fringe widths are constant over the whole interferogram. However, for asymmetric spectra, the fringe width in the interferogram varies slightly for increasing longitudinal shifts of the wave packets. By Fourier analysis of such an interferogram the spectrum can be recovered in a unique way.

"Visibility-spectroscopy" of electron waves. In the following model experiment, the spectrum of a field emission electron gun has been measured. The contrast of the interference fringes was recorded quantitatively as a function of the longitudinal shift in the whole interference field consisting of about 15 000 fringes for the experimental parameters used in our low voltage interferometer (a few keV of total energy of the field emitted electrons at an energy spread of about 0.4 eV). This has been done by recording the whole interference field in sets of, e.g., 10 fringes successively with our CCD-camera densitometer. The digitized data sets were corrected for the (small) cylinder-lens action of the Wien filter, put together with matched phases in a personal computer and subsequently transferred to a VAX computer for Fourier analysis. In the first experiment [58, 59] a resolution of about 0.6 eV was obtained. The state of the art is now about 80 meV [60]. As an example, the energy spectrum of field emitted electrons measured by this method is given in Figure 8.

This result was obtained by taking into account 12 300 interference fringes with a contrast of $\geq 10\%$. About 2 000 low contrast fringes were neglected, which results in an error of less than 40 meV of the full width at half maximum of the spectrum given in Figure 7. The total error of 80 meV contains 40 meV of error due to sampling of data (which can be largely avoided in future experiments). It is caused by

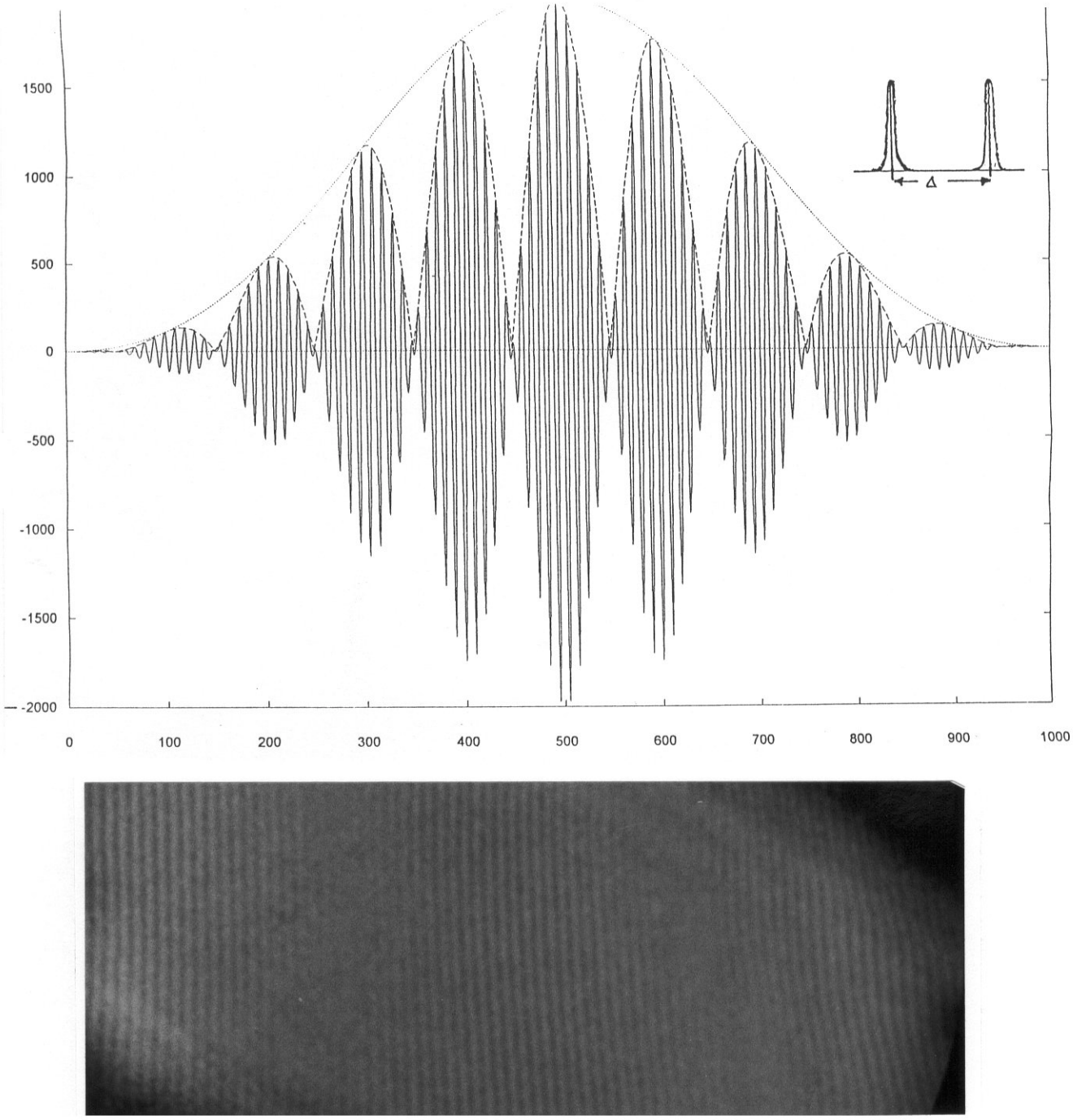

Figure 7. (**a**) Computer simulation of an interferogram of a spectrum consisting of two Gaussian shaped spectral lines of equal intensity separated by an energy Δ (see inset). (**b**) Electron interferogram corresponding to the central part of the simulated interferogram in (a). The energy of the electron "lines" was 1700 eV and 1722 eV (ΔE = 22 eV). Two regions of vanishing fringe contrast are clearly visible.

the fact that from the recorded 128 sample points per fringe only 16 sample points per fringe could be used for Fourier transformation due to the limited main memory of the VAX computer. This resolving power of 80 meV surpasses by far, that of electron spectrometers which are used in today's analytical electron microscopes. Their resolution is limited

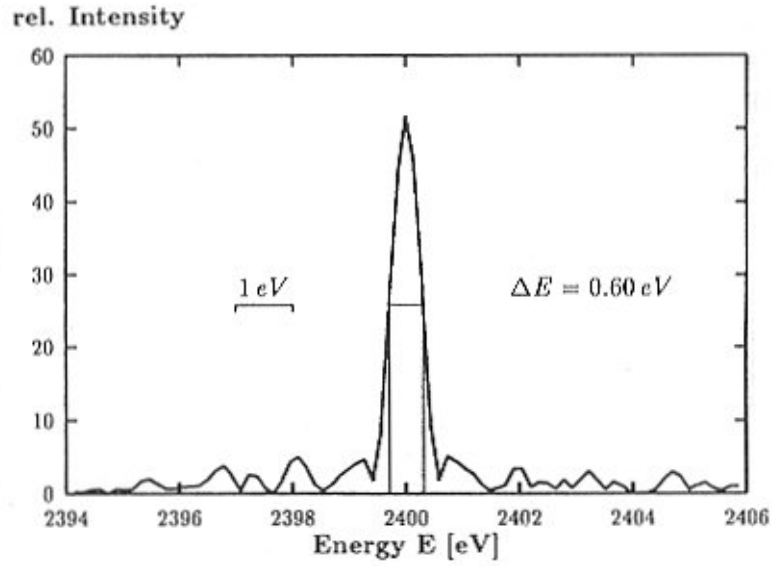

Figure 8. Spectrum of a field electron emitter obtained by Fourier analysis; total energy of the electrons: 2.4 keV.

by the source energy width to about 0.5 eV. Therefore, the high resolution that can be achieved by this method seems to make no sense on a first glance. With future monochromatized field emission electron sources or sources with intrinsic smaller energy width, as described in the section on Fermion anticorrelations (below), this situation will change. In the moment magnetic spectrometers are definitely superior to Fourier spectroscopy since data acquisition time for one spectrum is typically 30 minutes for the present state. This time can be reduced to a few minutes by further automation in future. Another dramatic reduction can be achieved by measuring contrast for each 20th fringe only and approximating the exact contrast function by this coarse grained one. A further step of data reduction is possible if some information on the spectrum that is to be measured is available *a priori*. For example, when the spectrum consists of two lines only. Then the energetic separation of the two lines can be calculated just by evaluating the distance of the contrast maxima in the interference pattern.

The Fourier transform spectrometer presented here is the *first spectrometer for particles that relies fully on quantum mechanics, i.e., the wave properties of matter*. It seems remarkable that this experiment proves that the *quantum mechanical probability waves* exhibit the same features as the "real" waves, e.g., of an electromagnetic field. All *conventional* spectrometers for charged particles are based on the dispersion of particle trajectories in electromagnetic fields.

Status of New Experiments, Perspectives

Ion interferometry

The remarkable insensitivity of the new interferometer to vibrations makes it seem likely that an interferometer for ions with their even shorter wavelengths can be realized. A biprism interferometer for ions, which are of course charged particles, is a welcome supplement to the rapidly developing field of interferometry with neutral atoms [15, 64, 65, 101, 110]. Its experimental potential may prove to be as valuable, or even more valuable than that of atom interferometers: For ions, powerful optical elements need not be developed. High brightness field ion sources, liquid metal sources and ion sources with single atom tips [37, 38, 95, 96, 106] are already available. The key elements, such as lenses, deflectors, mirrors, and beam splitters, are available (based on 50 years of experience in charged particle optics).

The most attractive feature of ion interferometer is the enormous phase sensitivity caused by the high rest masses of these particles. In addition to the high phase sensitivity and the inner degrees of freedom, features that ions have in common with atoms, these *composite* charged particles interact with electromagnetic potentials. Therefore, for the first time, aspects of the interaction of scalar- and vector-potentials (Aharonov-Bohm effects) in relation to the inner structure of the particles, fundamental for the understanding of gauge invariance, can be tested. The electric Aharonov-Bohm effect [1, 92], which has not yet been experimentally confirmed even for electrons due to the extremely fast switching of potentials necessary for these light particles, could be realized with protons and composite ions. The high phase sensitivity will allow the realization of inertial and gravitational sensors of unprecedented precision and in turn novel experiments to test relativity. Additionally, their inner degrees of freedom render possible a new class of interferometric experiments.

The aim of our present experiments is to demonstrate diffraction at an edge and biprism interferences of protons, H_2^+-, D_2^+- and $^4He^+$ ions as first steps towards ion

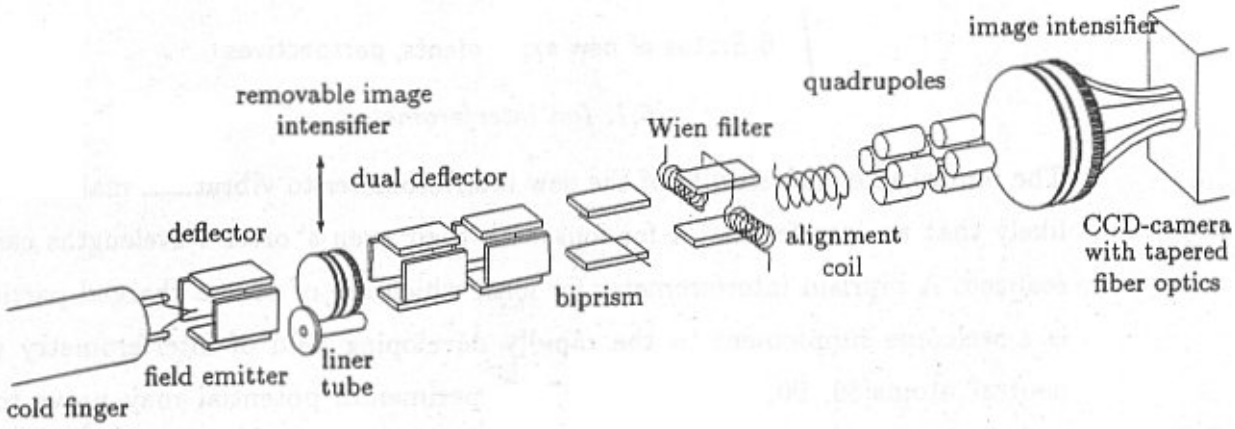

Figure 9. Experimental set-up.

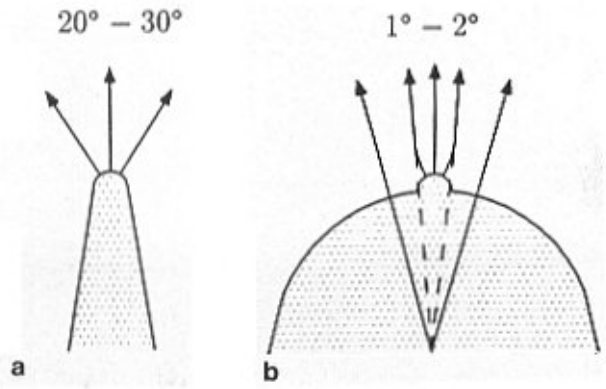

Figure 10. Electric field in front of a conventional field emitter (**a**) and one with a "supertip" (**b**). The emission is confined by the supertip geometry to a substantially smaller angle compared to a conventional tip.

---

interferometry. In an ion interferometer disturbances have to be very carefully avoided, since the wavelength and therefore the spacings between the interference fringes even for protons are expected to be about 45 times smaller than for electrons of the same kinetic energy. The salient point of the ion biprism interferometer under development is that it can be switched from electron interferometry to positively charged ion interferometry, simply by reversing the voltages of all the optical components and running the field emitter as a gaseous field-ion source. All optical components are electrostatic, apart from some coils which generate homogeneous fields for alignment purposes, e.g., for rotating the wavefront direction slightly. The electrostatic principle guarantees that the alignment for ions can be done very efficiently with a high intensity field electron beam.

As a highly coherent field emission source of electrons, protons, H_2^+- and He^+-ions we use a single, specially treated "supertip", cooled down during operation to 77 K or even to 10 K in order to achieve sufficient brightness. The "supertip" (Fig. 10b), a protrusion consisting of a small number of tungsten atoms on an <111>-oriented tungsten field emission tip with a relatively large radius of curvature of the apex, is prepared *in situ* in the interferometer. It is prepared by modifying the procedure first described by Hanson and Schwoebel [51, 52, 108, 109]. The preparation process of the "supertip" involves heating to about 1000 K and cooling of the tip to about 77 K [56, 63]. A coolable imaging gas inlet is mandatory in order to pursue the "supertip" formation process field-ion-microscopically and to enhance the brightness of the field-ion source. The emission pattern is observed on the screen of a channelplate image intensifier via a mirror (not drawn in Fig. 9), which can be inserted between the ion gun and the interferometer. The present source emits ions and electrons into single spots of an angular diameter of about 1°, (Fig. 11) compared to about 20° for very sharp single- or few-atom "nanotips" (Fig. 10a). The confinement of the ions into the small emission angle leads to the desired higher angular current.

Fortunately, the typical onset voltage is rather low for this kind of tip: about 350 V for electron- and 2-4 kV for ion-emission. The first deflector behind the field emitter is used to align the beam to the direction of the optic axis of the interferometer. After preparation of the supertip, the image intensifier is removed from the beam path and the ions (or electrons) are injected through a shielding tube into the interferometer. The second (double) deflector is for aligning the beam on to the optic axis of the biprism interferometer.

Again, by appropriate excitation of the electric and magnetic fields of the Wien filter, longitudinal shifts of the wave packets, which inevitably occur when the latter transverse electrostatic fields spatially separated, e.g., in the deflectors, are compensated. Thus, longitudinal

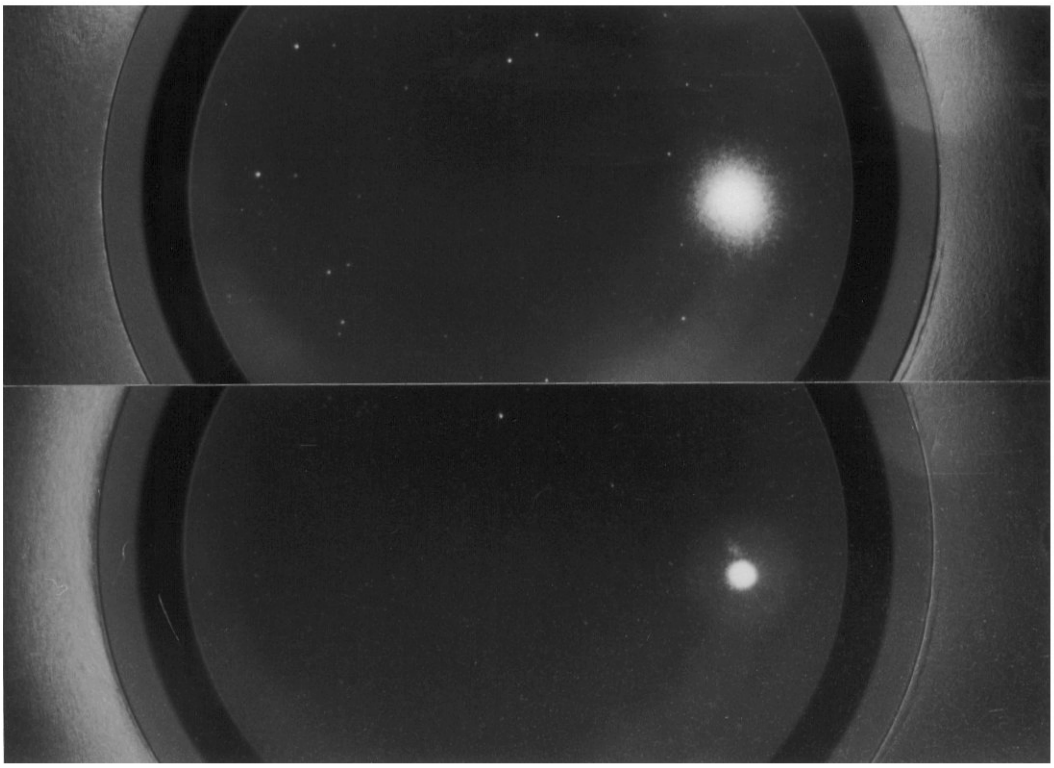

Figure 11: Emission pattern of a "supertip". The confinement of the emission into angles of the order of a few resp. about 1 degree is demonstrated for electron emission (top) and ion emission (bottom).

coherence is optimized in the plane of interference or even restored, if it was lost totally due to different group velocities in the electric field of the deflectors [89].

The fringe spacings in the primary interference pattern behind the biprism are expected to be 2 to 20 nm. Therefore, in order to adapt the spacings to the resolution of the channelplate detector, the pattern has to be magnified about 10000 times. For this purpose we use electrostatic quadrupole lenses, since they provide strong line focusing with different, very short focal lengths in two orthogonal planes. This is very advantageous for the magnification of interference fringes, since this feature allows one to magnify the fringe distance and simultaneously compress the fringes in perpendicular direction, i.e., along the fringe direction. This leads to a substantial gain in current density in the detection plane.

State of the art of ion interferometry. The actual set-up works well as an electron interferometer, but fails at present to detect ion interferences. The main reason for this failure is the low emitted ion current, which, combined with very high magnification, leads to poor current density in the detection plane. While the dual-stage channelplate image intensifier with a P20-phosphorus allows one to detect single electron and ion impacts without adding substantial noise, the previously used (TV-frequency) CCD camera-system created a substantial amount of noise internally, if on-chip exposure exceeded a few minutes. Recently, we were able to overcome these problems by using a cooled "state of the art" slow-scan CCD camera-system, which accepts exposure times up to 1 hour. Combining the new camera system with our interferometer will, we hope, be the only additional step necessary towards the realization of ion interferometry. [*Note*: In the meantime we observed diffraction at both edges of the biprism filament and biprism interferences with helium ions. It is planned to publish these results in Phys Rev Lett].

In addition to on-chip integration in the camera, image processing of the fringe pattern is provided by a personal computer in order to improve the signal to noise ratio: With the image rotation coil the fringe pattern is exactly aligned parallel to one direction of the array of pixels of the CCD-sensor. The events stored in a pixel column (or row) are integrated in the PC to give an improved signal to noise ratio in the resulting densitometer traces.

Fermion anticorrelations

In 1956 R. Hanbury Brown and R.Q.Twiss [48, 49, 50, 73] reported their, at the time, spectacular finding of

Table 2. Beam degeneracies and brightness of electron guns.

	standard field emission microscope	diode electron gun
degeneracy	10^{-6}	5.10^{-5}
energy	10^5 eV	10^3 eV
ΔE	0.3 eV	0.3 eV
Brightness B	10^8 A cm^{-2} sr^{-1}	10^8 A cm^{-2} sr^{-1}

correlations in the fluctuations of two photoelectric currents provoked by coherent beams of light. The mean square fluctuation in these photoelectric currents was twice that predicted for classical (Boltzmann-) particles and may be explained by interference between the two wave trains: In an intense photon beam there exists a certain probability that two photons arrive simultaneously at the photocathode, i.e., the photon wave packets overlap. The probability p for the generation of a photoelectron is proportional to the square of the amplitude: $p \infty A^2$; for constructive interference 4 photoelectrons are generated, for destructive their number is 0. Evidently, the resulting fluctuations in a coherent field of bosons are twice as large as for the arrival of classical particles. If we replace the photon beams in an experiment by coherent beams of electrons, the Pauli principle does not allow two electrons to be in the same quantum mechanical state (a single phase space cell); in other words, accidentally overlapping wave trains are not allowed (wave function antisymmetrization). In a coherent field of electrons, within the coherence time τ_c no second electron is allowed to arrive (antibunching). Consequently, the fluctuations in a coherent field of electrons are smaller than for classical particles. Therefore, the illumination of an area by fermions is, in principle, more uniform [107] and since the arrival time intervals between single electrons is $\geq \tau_c$ there exists a lower limit of lateral distance between the electrons. The interaction between the electrons and consequently the anomalous energy broadening [11] in a coherent polarized beam of electrons is reduced drastically. Rose and Spehr [102, 103] calculated that by using a totally polarized electron beam, which is required in order to enforce the existence of the lower lateral distance limit between the electrons, the anomalous broadening in a typical electron optical set-up is reduced to about 4% compared to an unpolarized beam (for electrons in different spin states there exists no lower limit for the impact parameter). The interaction between the particles in an unpolarized intense beam produces the well known anomalous energy widths [11].

An electron antibunching experiment. The only candidate for testing fermion antibunching is electrons [111-116, 128] because for heavier particles the beam degeneracies of the available sources are hopelessly small. The beam degeneracy δ means the ratio of the actual brightness of the emitter (occupation number per cell in phase space) to the theoretical maximum brightness B_{max} (by Pauli's exclusion principle the maximum occupation per cell is two for fermions with opposite spin directions) [44, 45, 129, 130].

$$B_{\max} = \left(\frac{4me}{\hbar^3}\right) E\Delta E \qquad (3)$$
$$= 5.2\_10^9\, E(eV)\, \delta\, E(eV)\,(A cm^2\, sr^{-1})$$

The beam degeneracy δ of the electron beam in a standard field emission electron microscope is given according to Silverman [114] in Table 2.

With our low-aberration diode field-emission gun, a brightness of the same order as for the microscope given above at 1 keV seems realistic. [*Note*: Eventually, if the brightness of our gun turns out to be much smaller than given in the table, it could be enhanced by using a "supertip" as described in the chapter on ion interferometry and/or using a EuS-coated tip (see the section on "Polarized electron source")]. Consequently, the beam degeneracy of about 5.10^{-5} is nearly two orders of magnitude larger and compares quite favorably with that of 10^{-3}, which was available in the classical Hanbury Brown and Twiss experiment.

In our experiment, two electron detectors in the interference plane of the interferometer measure coincidences of the arrival times of electrons. The time resolution of the fast coincidence will be of the order of 10^{-10} seconds [20, 21, 22, 127], which is 4 orders of magnitude less than the theoretically required resolution given by the coherence time τ_c in order to see that no two electrons arrive within the coherence time. Having a resolution of 10^{-10} seconds only, we expect to measure a random coincidence rate reduced by a factor of 1.10^{-4} since within the first 10^{-14} seconds after the arrival of an electron no second one arrives due to the Pauli principle. This causes the reduction of random coincidences in a coherent electron beam. In conclusion,

antibunching of electrons should be observable with our electron interferometer and presently available technology of fast coincidence counting.

Polarized electron source

Ferromagnetic EuS-coated tungsten field emitter tips emit below the Curie temperature of about 16.5 K of EuS and, after a very special annealing, a 90% polarized electron beam with an energy spread of 80 meV only [66]. One reason for this exceptionally small energy width may be the reduced interaction due to antibunching of electrons at the cathode. Their brightness has not yet been measured but, at low temperatures according to the data given by Kisker *et al*. [66], it seems to exceed that of a tungsten field emitter by one or two orders of magnitude. This source, first developed by Müller and coworkers [88] and applied to problems in atomic physics [66], is most promising for electron interferometry, electron anticorrelation measurements, electron microscopy and even more for spin-resolved scanning tunnelling microscopy (highly resolved imaging of ferromagnetic domains) and spectroscopy.

Acknowledgements

My colleagues Dr. Marc Nicklaus, Andreas Schäfer, Uwe Maier, Harald Kiesel, Hubert Kraus, Matthias Bauer, Dr. R. Neutze and Tomas Tyc are gratefully acknowledged for helpful discussions. The study was financially supported by the Deutsche Forschungsgemeinschaft (Ha 1063/2, Ha 1063/7, Ha 1063/11, Ha 1063/15).

References

1. Aharonov Y, Bohm D (1959) Significance of electromagnetic potentials in the quantum theory. Phys Rev **115**: 485-491.

2. Anonymous (1974) High voltage, high resolution microscopes. Physics Today, May 1974, 17-18.

3. Bauer M (1994) Interferometrische Untersuchung der Kohärenzeigenschaften einer mittels Wien-Filter monochromatisierten Feldemissionselektronenquelle (Interferometric investigation of the coherence properties by a Wien-filter monochromatized field emission electron source). Master's Thesis, University of Tübingen.

4. Bauer M, Hasselbach F (1995) A monochromatized field electron source. Optik **100** Suppl **6**: 7

5. Bayh W (1962) Messung der kontinuierlichen Phasenschiebung von Elektronenwellen im kraftfeldfreien Raum durch das magnetische Vektorpotential einer Wolfram-Wendel (Measurement of the continuous phase shift in force-free space by the magnetic vector potential of a tungsten coil). Z Phys **169**: 492-510.

6. Beck A (1989) Optimierung von Transmissions-photokathoden für Röntgenbildwandler mit einer Auflösung von 100 nm bei 4,5 keV Primärstrahlung (Optimization of transmission photo cathodes for X-ray images with a resolution of 100 nm at 4.5 keV primary radiation). Doctoral Thesis, University of Tübingen.

7. Bernstein HJ, Low FE (1987) Measurement of longitudinal coherence lengths in particle beams. Phys Rev Lett **59**: 951-953.

8. Boersch H (1940) Fresnelsche Elektronenbeugung (Fresnel electron diffraction). Naturwissenschaften **28**: 709-711.

9. Boersch H (1940) Randbeugung von Elektronen (Edge diffraction of electrons). Physik Z **44**: 32-38.

10. Boersch H (1943) Fresnelsche Beugung im Elektronenmikroskop (Fresnel diffraction in the electron microscope). Physik Z **44**: 202-211.

11. Boersch H (1954) Experimentelle Bestimmung der Energieverteilung in thermisch ausgelösten Elektronenstrahlen (Experimental determination of the energy distribution in thermally induced electron beams). Z Physik **139**: 115.

12. Boersch H, Hamisch H, Grohmann K (1962) Experimenteller Nachweis der Phasenschiebung von Elektronenwellen durch das magnetische Vektorpotential (Experimental proof of phase shift of electron waves by the magnetic vector potential). Z Phys **169**: 263-272.

13. Brünger W (1968) Feldemissionskathode zur kohärenten Beleuchtung des Elektronen-Biprismas (Field emission cathode for coherent illumination of the electron biprism). Naturwissenschaften **55**: 295-296.

14. Buhl R (1959) Interferenzmikroskopie mit Elektronenwellen (Interference microscopy with electron waves). Z Phys **155**: 395-412.

15. Carnal O, Mlynek J (1991) Young's double slit experiment with atoms: A simple atom interferometer. Phys Rev Lett **66**: 2689-2692.

16. Chambers RG (1960) Shift of an electron interference pattern by enclosed magnetic flux. Phys Rev Lett **5**: 3-5.

17. Chiao RY (1990) Geometrical and topological (an)holonomies in optical experiments. In: Quantum Coherence, Proceedings of the International Conference on Fundamental Aspects of Quantum Theory to Celebrate 30 Years of the Aharonov-Bohm Effect. Anandan JS (ed). World Scientific, Singapore. pp 107-121.

18. Comsa G (1987) Comment on "Longitudinal coherence in neutron interferometry". Phys Rev **58**: 2274.

19. Cosslett VE (1954) Present trends in electron microscopy. Proc NBS Semicentennial Symposium on Electron Physics. NBS Circular 527 (March 17th, 1954). pp 291-303.

20. Cova S, Ghioni M, Zappa F (1990) Improving the performance of ultrafast microchannel-plate photomultipliers in time-correlated photon counting by pulse pre-shaping.

Rev Sci Instrum **61**: 1072.

21. Cova S, Ghioni M, Zappa F (1991) Optimum amplification of microchannel-plate photomultiplier pulses for picosecond photon timing. Rev Sci Instrum **62**: 2596.

22. Cova S, Ghioni M, Zappa F, Lacaita A (1993) Constant-fraction circuits for picosecond photon timing with microchannel plate photomultipliers. Rev Sci Instrum **64**: 118.

23. Crewe AV, Eggenberger DN, Wall J, Welter LM (1968) Electron gun using a field emission source. Rev Sci Instr **39**: 576-583.

24. Crewe AV, Wall J, Welter LM (1968) A high resolution scanning transmission electron microscope. J Appl Phys **39**: 5861-5868.

25. Daberkow I, Gauch H, Hasselbach F (1983) Measurement of the longitudinal coherence of electrons from a field emission source. Proc Joint Meeting on Electron Microscopy, Antwerp. Published by Soc Belge de Microsc Electronique and Deutsche Gesellschaft für Elektronenmikroskopie. p 100.

26. Davisson C, Germer LH (1927) Scattering of electrons by a single crystal of nickel. Nature **119**: 558-560.

27. de Broglie L (1923) Radiation - Ondes et quanta (Radiation: waves and quanta). C R Acad Sci Paris **177**: 507-510.

28. de Broglie L (1923) Waves and quanta. Nature **112**: 540.

29. de Broglie L (1924) A tentative theory of light quanta. Phil Mag **47**: 446-458.

30. Dieks D (1990) A quantum mechanical twin paradox. Found Physics Letters **3**: 347-357.

31. Dieks D, Nienhuis G (1990) Relativistic aspects of nonrelativistic quantum mechanics. Am J Phys **58**: 650-655.

32. Drahos V, Delong A (1964) The source width and its influence on interference phenomena in a Fresnel electron biprism. Opt Acta **11**, 173-181.

33. Ehrenberg W, Siday RE (1949) The refractive index in electron optics and the principle of dynamics. Proc Phys Soc **62**: 8-21.

34. Elsasser W (1925) Bemerkungen zur Quantenmechanik freier Elektronen (Remarks on the quantum mechanics of free electrons). Naturwissenschaften **13**: 711.

35. Esterman I, Stern O (1930) Beugung von Molekularstrahlen (Diffraction of molecular beams). Z Physik **61**: 95-125.

36. Faget J, Fert C (1957) Diffraction et interférences en optique électronique (Diffraction and interference in electron optics). Cah Phys **83**: 286-296.

37. Fink HW (1986) Mono-atomic tips for scanning tunneling microscopy. IBM J Res Develop **30**: 460-465.

38. Fink HW (1988) Point source for ions and electrons. Physica Scripta **38**: 260-263.

39. Franz W (1939) Elektroneninterferenzen im Magnetfeld (Electron interference in the magnetic field). Verh D Phys Ges **20**: 65-66.

40. Franz W (1940) Elektroneninterferenzen im Magnetfeld (Electron interference in the magnetic field). Physikal Berichte **21**: 686.

41. Gabor D (1948) A new microscopic principle. Nature **197**: 777-778.

42. Gabor D (1949) Microscopy by reconstructed wave-fronts. Proc R Soc A **197**: 454-487.

43. Gabor D (1951) Microscopy by reconstructed wave-fronts II. Proc R Soc B **64**: 449-469.

44. Gabor D (1961) Light and Information. In: Progress in Optics. Wolf E (ed). North Holland, Amsterdam. Vol 1, pp 109-153.

45. Goldberger ML, Lewis HW, Watson KM (1963) Use of intensity correlation to determine the phase of scattering amplitude. Phys Rev **132**: 2764-2787.

46. Haine ME, Dyson J (1950) A modification to Gabor's proposed diffraction microscope. Nature **166**: 315-316.

47. Haine ME, Mulvey T (1954) Problems in the realization of diffraction microscopy with electrons, Proc NBS Semicentennial Symposium on Electron Physics. NBS Circular 527 (March 17th, 1954). pp 247-250.

48. Hanbury Brown R, Twiss RQ (1957) Interferometry of the intensity fluctuation in light. Proc Roy Soc London **242**: 300-324.

49. Hanbury Brown R, Twiss RQ (1958) Interferometry of the intensity fluctuation in light. Proc Roy Soc London **243**: 291-319.

50. Hanbury Brown R, Twiss RQ (1974) The Intensity Interferometer. Taylor and Francis Ltd, London.

51. Hanson G, Schwoebel P (1986) Cathode bombardment stimulated microstructure growth - average ion energy. J Physique C2 **47**: 59-66.

52. Hanson GR, Siegel BM (1979) H_2 and rare gas field ion source with high angular current. J Vac Sci Technol **16**: 1176.

53. Hasselbach F (1979) Ein kleines UHV-Biprisma-Elektroneninterferometer für 2 keV Elektronen (A small UHV-biprism electron interferometer for 2 keV electrons). 19. Tagung der Deutschen Gesellschaft für Elektronenmikroskopie, Tübingen 1979, Abstract 7L1. Published by Deutsche Gesellschaft für Elektronenmikroskopi. p. 90.

54. Hasselbach F (1988) A ruggedized miniature UHV electron biprism interferometer for new fundamental experiments and applications. Z Phys B - Condensed Matter **71**: 443-449.

55. Hasselbach F (1995) Experiments with coherent electron wave packets. In: Fundamental Problems in Quantum Physics. Ferrero M, van der Merve A (eds). Kluwer

Academic Publishers, Dordrecht. pp 123-139.

56. Hasselbach F, Kraus H (1995) Development of a bright, highly coherent field ion source. Optik Suppl **100**: 6.

57. Hasselbach F, Nicklaus M (1993) Sagnac experiment with electrons: Observation of the rotational phase shift of electron waves in vacuum. Phys Rev A **48**: 143-151.

58. Hasselbach F, Schäfer A (1990) Interferometric (Fourier-spectroscopic) measurement of electron energy distributions. Proc 12th Int Congress on Electron Microscopy. Peachey LD, Williams DB (eds). San Francisco Press, San Francisco. Vol 2, pp 110-111.

59. Hasselbach F, Schäfer A (1993) Einrichtung zur interferometrischen (fourierspektroskopischen) Messung der Energieverteilung geladener Teilchen. [Instrument for the interferometric (Fourier spectroscopic) determination of the energy distribution of charged particles]. German Patent DE 40 24 624 A1.

60. Hasselbach F, Schäfer A, Wachendorfer H (1995) Interferometric measurement of charged particle spectra (Fourier-spectroscopy). Nucl Instr Meth Phys Res A **363**: 232-238.

61. Hawkes PW (1978) Coherence in electron optics. Adv Opt Electron Microsc **7**: 101-184.

62. Hendriks BHW, Nienhuis G (1990) Sagnac effect as viewed by a co-rotating observer. Quantum Opt **2**: 13-21.

63. Jousten K, Böhringer K, Börret R, Kalbitzer S (1988) Growth and current characteristics of stable protrusions on tungsten field ion emitters. Ultramicroscopy **26**: 301-311.

64. Kasevich M, Chu S (1991) Atomic interferometry using stimulated Raman transitions, Phys Rev Lett **67**: 181-184.

65. Keith DW, Eckstrom CR, Turchette QA, Prichard DE (1991) An interferometer for atoms. Phys Rev Lett **66**: 2693-2696.

66. Kisker E, Baum G, Mahan AH, Raith W, Reihl B (1978) Electron field emission from ferromagnetic europium sulfide on tungsten. Phys Rev B **18**: 2256-2275.

67. Klein AG, Opat GI, Hamilton WA (1983) Longitudinal coherence in neutron interferometry. Phys Rev Lett **50**: 563-565.

68. Komrska J, Vlachova B (1973) Justification of the model for electron interference produced by an electrostatic biprism. Opt Acta **20**: 207-215.

69. Komrska J, Drahos V, Delong A (1964) Fresnel diffraction of electrons by a filament. Opt Acta **11**: 145-157.

70. Komrska J, Drahos V, Delong A (1967) Intensity distributions in electron interference phenomena produced by an electrostatic biprism, Opt Acta **14**: 147-167.

71. Leavitt JA, Bills FA (1969) Single slit diffraction pattern of a thermal atomic potassium beam. Am J Phys **37**: 905-912.

72. Lin JA, Cowley JM (1986) Calibration of operating parameters for HB5 STEM instrument. Ultramicroscopy **19**: 31- 42.

73. Mandel L (1963) Fluctuation of light beams. In: Progress in Optics. Wolf E (ed). North Holland, Amsterdam. Vol 2, p 181-248.

74. Mankos M, Cowley JM, Scheinfein MR (1996) Quantitative micromagnetics at high spatial resolution using far-out-of-focus STEM electron holography. Phys stat solidi (a) **154**: 469-504.

75. Marton L (1952) Electron interferometer. Phys Rev **85**: 1057-1058.

76. Marton L, Simpson JA, Suddeth JA (1954) An electron interferometer. Rev Sci Instr **25**: 1099-1104.

77. Marton L, Simpson JA, Suddeth JA (1954) An electron beam interferometer. Phys Rev **90**: 490-491.

78. Michelson AA (1891) Visibility of interference-fringes in the focus of a telescope. Phil Mag **31**: 256-259.

79. Michelson AA (1891) On the application of interference methods to spectroscopic measurements I. Phil Mag **31**: 338-346.

80. Michelson AA (1892) On the application of interference methods to spectroscopic measurements II. Phil Mag **34**: 280-299.

81. Missiroli GF, Pozzi G, Valdrè U (1981) Electron interferometry and interference electron microscopy. J Phys E: Sci Instrum **14**: 649-671.

82. Möllenstedt G, Bayh W (1962) Kontinuierliche Phasenschiebung von Elektronenwellen im kraftfeldfreien Raum durch das magnetische Vektorpotential eines Solenoids (Continuous phase shift of electron waves in force-free space by the magnetic vector potential of a solenoid). Physikalische Blätter **18**: 299-305.

83. Möllenstedt G, Düker H (1955) Fresnelscher Interferenzversuch mit einem Biprisma für Elektronenwellen (Fresnel interference experiments with a biprism for electron waves). Naturwissenschaften **42**: 41.

84. Möllenstedt G, Düker H (1956) Beobachtungen und Messungen an Biprisma-Interferenzen mit Elektronenwellen (Observations and measurements on biprism interferences with electron waves). Z Phys **145**: 377-397.

85. Möllenstedt G, Keller M (1957) Elektroneninterferometrische Messung des inneren Potentials (Electron interferometric measurement of the inner potential). Z Phys **148**: 34-37.

86. Möllenstedt G, Wahl H (1968) Elektronenholographie und Rekonstruktion mit Laserlicht (Electron holography and reconstruction with laser light). Naturwissenschaften **55**: 340-341.

87. Möllenstedt G, Wohland G (1980) Direct interferometric measurement of the coherence length of an electron wave packet using a Wien filter. Electron Microscopy 1980, Brederoo P, Boom G (eds). Seventh

European Congress on Electron Microscopy Foundation, Leiden. Vol 1, pp 28-29.

88. Müller M, Eckstein W, Heiland W, Zinn W (1972) Electron spin polarization in field emission from EuS-coated tungsten tips. Phys Rev Lett **29**: 1651.

89. Nicklaus M, Hasselbach F (1993) Wien Filter: A wave-packet-shifting device for restoring longitudinal coherence in charged-matter-wave interferometer. Phys Rev A **48**: 152-160.

90. Nicklaus M, Hasselbach F (1995) Experiments on the influence of electro-magnetic and gravito-inertial potentials and fields on the quantum mechanical phase of matter waves. Ann N Y Acad Sci **755**: 877-879.

91. Olariu S, Popescu II (1985) The quantum effects of electromagnetic fluxes. Rev Mod Phys **57**: 339-436.

92. Peshkin M, Lipkin HJ (1995) Topology, locality, and Aharonov-Bohm effect with neutrons. Phys Rev Lett **74**: 2847-2850.

93. Peskin M, Tonomura A (1989) The Aharonov-Bohm effect. Lecture Notes in Physics, Vol. 340, Springer Verlag, Berlin.

94. Post EJ (1967) Sagnac effect. Rev Modern Phys **39**: 475-493.

95. Qian W, Scheinfein MR, Spence JCH (1993) Electron optical properties of nanometer field emission electron sources. Appl Phys Lett **62**: 315-317.

96. Qian W, Scheinfein MR, Spence JCH (1993) Brightness measurements of nanometer-sized field-emission-electron sources. J Appl Phys **73**: 7041-7045.

97. Rang O (1964) Zur Eichtransformation der Elektronenwelle (On the calibration transformation of the electron wave) Optik **21**: 59-65.

98. Rang O (1977) Is the electron wavelength an observable? Ultramicroscopy **2**: 149-151.

99. Rauch H, Treimer W, Bonse U (1974) Test of a single crystal neutron interferometer. Phys Lett **47A**: 369-371.

100. Riehle F, Kisters T, Witte A, Helmcke J, Bordé CJ (1991) Optical Ramsey spectroscopy in a rotating frame: Sagnac effect in a matter-wave interferometer. Phys Rev Lett **67**: 177-180.

101. Riehle F, Witte A, Kisters T, Helmcke J (1992) Interferometry with Ca atoms. Appl Phys B **54**: 333-340.

102. Rose H, Spehr R (1980) On the theory of the Boersch effect. Optik **57**: 339-364.

103. Rose H, Spehr R (1983) Energy broadening in high-density electron and ion beams: The Boersch effect. Adv Electronics Electron Phys Suppl **13C**: 475-530.

104. Rubens H, Wood RW (1911) Focal isolation of long heat-waves. Phil Mag **34**: 280-299.

105. Schäfer A (1990) Fourierspektroskopie mit Elektronenwellen (Fourier spectroscopy with electron waves). Master's Thesis. Institut für Angewandte Physik, University of Tübingen.

106. Scheinfein MR, Qian W, Spence JCH (1993) Aberration of emission cathodes: nanometer diameter field-emission electron sources. J Appl Phys **73**: 2057-2068.

107. Scherzer O (1980) Wie gleichmässig kann man eine Fläche bestrahlen? (How evenly can one irradiate a surface?) Optik **56**: 333-352.

108. Schwoebel P, Hanson G (1984) Localized field ion emission using adsorbed hydrogen films on ⟨110⟩-oriented tungsten field emitters. J Appl Phys **56**: 2101-2105.

109. Schwoebel P, Hanson G (1985) Beam current stability from localized emission sites in a field ion source. J Vac Sci Technol **B3**: 215-219.

110. Shimizu F, Shimizu K, Takuma H (1991) Double-slit interference with ultracold metastable neon atoms. Phys Rev A **46**: R17-R20.

111. Silverman MP (1987) Fermion ensembles that show statistical bunching. Phys Lett A **124**: 27-31.

112. Silverman MP (1987) Distinctive quantum features of electron intensity correlation interferometry. Il Nuovo Cimento **97B**: 200-219.

113. Silverman MP (1987) Second order temporal and spatial coherence of thermal electrons. Il Nuovo Cimento **99**: 227-245.

114. Silverman MP (1987) On the feasibilitity of observing electron antibunching in a field-emission beam. Phys Lett A **120**: 442-446.

115. Silverman MP (1988) Application of photon correlation technique to fermions. In: OSA Proc Photon Correlation Techn and Applications. Abbiss JB, Smart AE (eds). OSA Washington, DC. Vol 1, pp 26-34.

116. Silverman MP (1988) Quantum interference effects on fermion clustering in a Fermion interferometer. Physica B **151**: 291-297.

117. Simpson JA (1954) The theory of the three-crystal electron interferometer. Rev Sci Instr **25**: 1105-1109.

118. Simpson JA (1956) Electron interference experiments. Rev Mod Phys **28**: 254-260.

119. Tomita H, Matsuda T, Komoda T (1970) Electron microholography by two beam method. Jap J Appl Phys **9**: 719.

120. Tonomura A (1969) Electron beam holography. J Electron Microsc **18**: 77-78.

121. Tonomura A (1987) Applications of electron holography. Rev Mod Phys **59**: 639-669.

122. Tonomura A, Osakabe N, Matsuda T, Kawasaki T, Endo J, Yano S, Yamada H (1986) Evidence for Aharonov-Bohm effect with magnetic field completely shielded from electron wave. Phys Rev Lett **56**: 792-795.

123. Tonomura A, Allard LF, Pozzi G, Joy DC, Ono YA (eds) (1995) Electron Holography, Proceedings of the International Workshop on Electron Holography, Knoxville, TN. North-Holland Delta Series, Elsevier, Amsterdam.

124. Wachendorfer H (1993) Fourierspektroskopie mit Elektronenwellen (Fourier spectrospcopy with electron waves). Master's thesis. Institut für Angewandte Physik, University of Tübingen.

125. Werner SA, Staudemann JL, Collela R, Effect of earth's rotation on the quantum mechanical phase of the neutron. Phys Rev Lett **42**: 1103-1106.

126. Wohland G (1981) Messung der Kohärenzlänge von Elektronen im Elektroneninterferometer mit Wien-Filter (Measurement of the coherence length of electrons in an electron interferometer with a Wien-filter). Doctoral Thesis, University of Tübingen.

127. Yamazaki I, Tamai N, Kume H, Tsuchiya H, Oba K (1985) Microchannel-plate photomultiplier applicability to the time-correlated photon-counting method. Rev Sci Instrum **56**: 1187-1194.

128. Yurke B (1988) Interferometry with correlated Fermions. Physica B **151**: 286-290.

129. Zeitler E (1975) Coherence in scanning transmission microscopy. Scanning Electron Microscopy; 1975: 671-678.

130. Zeitler E (1987) Zusammenhänge, die mit der Kohärenz zusammenhängen. (Correlations having a relationship with coherence). Optik **77**: 13-14.

Discussion with Reviewers

J. Spence: The observation of Fresnel fringes using ions seem very difficult since the coherence width $X_c = \lambda/\theta$ is also 45 times less than for electrons of the same energy and source size ($\theta \approx d_s/2z$ is the semi-angle subtended by the source at a diffracting edge distance z from the source). Thus, 45 times fewer fringes will be seen for the same conditions of source size and beam energy, and it is difficult enough to obtain 45 electron fringes. To observe even one fringe, X_c must exceed the size of the first fringe $(2\lambda z)^{1/2}$, so that we require $d_s \leq (2\lambda z)^{1/2}$. Is it possible to obtain such a small ion source with brightness to satisfy this condition?
Author: One crucial point in our estimation of the feasibility of an ion interferometer is the assumption that the lateral dimensions of the virtual source of a field ion emitter can be made of the order of a few nanometers down to atomic dimensions. For protons of 10 keV of energy the wavelength $\lambda = 3.10^{-4}$ nm; z is about 0.1 m; d_s is assumed to be 1 nm; $X_c = \theta/\lambda \approx (\lambda 2z/d_s) = 6.10^{-5} = 60$ μm and $d_s = (2\lambda z)^{1/2} = (2.3.10^{-4}$ nm. 10^8 nm)$^{1/2}$ = 2.5 10^2 nm = 0.25 μm. Hence, $X_c \geq d_s$ is required. Ion optically, such small virtual source sizes seem possible since the field ion microscope resolves atoms easily while the field electron microscope's intrinsic resolution is worse by at least a factor of 10 due to the large Fermi energy in metals and the corresponding energy spread [131]. If longitudinal coherence should be reduced or even lost due to shifts of the wave packets by electrostatic optics, then we can restore it by applying the coherence reviving action of a crossed field analyzer. You are right concerning the remark on the brightness. Our experimental brightness in the moment of the order of 10^4 A/cm^2 which is much less than required and the published [63, 109] values of supertip sources. However, we have not yet varied all parameters to improve it and hope to overcome the brightness problem in the near future.

P.W. Hawkes: I do not understand the remark concerning the electric and magnetic Aharonov-Bohm phase shifts. The electron beam passing though the Wien filter is "continuous", the space is not multiply connected. The phase changes thus seem to be classical and the comment on the electric Aharonov-Bohm effect does not seem justified.
Author: The electron beam is divided by the biprism into two laterally separated wavepackets and travels through the Wien filter with some lateral separation. The coherent electron beams, which form the interference fringes in the primary interference plane enclose an area which is limited by the closed polygon connecting cathode, left edge of the biprism filament, point of superposition in the plane of interference, right edge of the biprism filament, cathode (if only one biprism filament is used). The magnetic flux of the Wien filter penetrating parts of this enclosed area causes an Aharonov-Bohm phase shift.

J.M. Cowley: In the spectrum of Figure 8, are the oscillatory sidebands significant, or are these the result of termination of the input data from the interference fringe measurements? The spectrum appears to be plotted in intervals of about 0.2 eV, which does not appear to be consistent with the accuracy of 40 meV of the width determination.
Author: The answer to the first question is yes. We did not use a Hanning window but a reactangular one (top hat). The spectrum in Figure 8 has been evaluated with a Fourier field size of 2^{18}. The best accuracy of about 40 meV requires a field size of 2^{21} which was used in our last experiments. The symmetrical form of the curve remains but looks smooth then.

J.M. Cowley: Do you have plans to apply your interferometer to the measurement of phase changes of electron waves in solids or measurements of the loss of longitudinal coherence associated with the energy spread accompanying inelastic scattering processes in solids? Your instrument would seem to be ideal for these purposes.
Author: Phase changes of electron waves in solids have been measured, e.g., by Möllenstedt and Keller [85] (measurement of inner potentials in solids). Since our interferometer has no specimen stage, measurements of the

loss of longitudinal coherence due to inelastic scattering processes in solids are not possible at the moment. One disadvantage of our interferometer for these measurements is that it works with very low energies (150 eV to 5 keV). Extremely thin specimens will be necessary. The most precise coherence length measurements available have been performed with this instrument. Contrast differences and changes of the fringe location of the order of a per cent are accessible with the computer controlled CCD-densitometer. We will bear in mind the interesting proposals including the problems raised in your paper on "chromatic coherence and inelastic scattering in electron holography" [132].

G. Pozzi: I greatly appreciated your outline of the action of the Wien filter; however, recalling the subtleties regarding the effects of electromagnetic fields on wavefunctions and wavepackets, I would like to know if there is a full quantum mechanical analysis of the problem.
Author: To my knowledge, no full quantum mechanical analysis exists. We are just beginning to carry it through.

T. Mulvey: You have succeeded in making a column that is remarkably resistant to the effects of external vibration and stray fields. Do you have any suggestions for the improvement of the design of electron optical columns, bearing in mind that most commercial electron microscopes cannot reach their guaranteed resolution during normal working hours?
Author: I appreciate this question very much since it gives me the possibility to accentuate the essentials of the new column design. Relative displacements of the components of high resolution columns are excited by vibrations coming from the floor of the building. These are accentuated when the mechanical eigenfrequency of the column approaches the frequency of these vibrations. Two counteractive cures exist: (*i*) Firstly, to keep the instrument clear of these vibrations. In state of the art microscopes this is done by passive systems with rather limited success, as is well known. An active approach seems to me much more promising: The x-, y-, and z-signals of a velocity sensing seismometer are digitized, filtered, integrated and retransformed into analog signals which actuate, e.g., piezotranslators and exactly compensate the deflections of the platform of the microscope, (*ii*) The second approach to the problem is to avoid vibrationally induced relative displacements of the electron optical components by suitable constructional measures. The displacements and in turn the disturbances decrease rapidly with increasing difference in the frequency of excitation, which is very low usually, and the mechanical eigenfrequency of the column. The solution of the problem is to trim the eigenfrequency to values as high as possible. This approach has been realized in our interferometer to such a degree that no vibration damping or isolation as described under (*i*) was necessary at all. Constructive essentials are: small lightweight components, stiff materials, no mechanical alignment facilities. These constructional principles are applicable for all instruments working up to about 30 kV, i.e., most scanning electron microscopes. I expect that there will be some problems to realize these principles in magnetic microscopes of 100 or more kV accelerating voltage, which require bulky lenses. Nevertheless, the electron source and the condenser lenses can be constructed much lighter than usual and the last projector lens can be omitted in favor of a very small single crystal, high DQE, miniature fluorescent screen coupled fiber optically to a 2x2 k-pixel CCD-sensor. These modifications will reduce the total mass of such a microscope substantially and increase in the mechanical eigenfrequency correspondingly.

The sensitivity of conventional columns to magnetic alternating current (AC)-fields is due to a rather inefficient shielding. Each electron optical component is shielded separately by a shield with a low diameter to length ratio. Stray fields penetrate between these separate shields into the column. Lateral bores for alignment of diaphragms or insertion of the specimen have an additional detrimental effect on the shielding factor. An effective shield consists of a long high permeability metal cylinder with a large diameter to length ratio, without any lateral bores, which is put on the entire column after insertion of the specimen *and alignment*. Leakage magnetic fields of the magnetic lenses of a column have to be carefully shielded from this high permeability shield in order not to drive it into saturation (this would cause a strongly reduced shielding factor of this outer shield). Our interferometer is shielded by a single high permeability cylinder. The contrast of the interference fringes is not affected when we switch on the fluorescent lamps in the lab, despite the fact that the interferometer is working with low energy electrons in the range of 150 eV to 2.5 keV. By combining effective shielding with approach (*i*) and (*ii*) substantial progress will be possible also in high voltage TEMs. In field emission electron microscopes, as in our Sagnac-interferometer, when all vibrational and phase shifting disturbances caused by variation of enclosed fluxes are eliminated, the temporal instabilities of the emission sites in the end limit the quality of the instrument.

Reviewer VI: Could an interferometer of this type be applied to the study of material properties? If so, what advantages would such an instrument have over conventional analytical instruments?
Author: The answer to the first part of the question is yes. However, some modifications are recommended/necessary: 1. A specimen stage. 2. If microscopic observation is necessary, the quadrupole lenses could be easily replaced by rotationally symmetric electrostatic lenses. Energy loss

spectroscopy of selected small areas of the specimen would be possible then by Fourier-spectroscopy as well as low energy in-line and off-axis holography and interference microscopy for solving material science problems (e.g., study of electromagnetic field distributions in specimens and near surfaces, convergent beam interferometry [133]. Very thin specimens are indispensable due to the low energy of the electrons.

Additional References

131. Brodie I (1978) The visibility of atomic objects in the field electron emission microscope. Surface Sci **70**: 186-196.

132. Cowley JM (1995) Chromatic coherence and inelastic scattering in electron holography. Ultramicroscopy **57**: 327-331.

133. Herring RA, Pozzi G (1995) Modeling of convergent beam interferometry. In: Electron Holography. Tonomura A, Allard LF, Pozzi G, Joy DC, Ono YA (eds). North-Holland Delta Series, Elsevier Science, Amsterdam. pp 287-296.